Formation of high entropy metal diborides using arc-melting and combinatorial approach to study quinary and quaternary solid solutions

Simone Failla[a], Pietro Galizia[a], Shuai Fu[b], Salvatore Grasso[b], Diletta Sciti[a]*

[a] CNR-ISTEC, National Research Council of Italy - Institute of Science and Technology for Ceramics, Via Granarolo 64, 48018, Faenza, Italy

[b] Key Laboratory of Advanced technologies of Materials, Ministry of Education, School of Materials Science and Engineering, Southwest Jiaotong, Chengdu 610031, China

*Corresponding authors: Prof. Salvatore Grasso, School of Materials Science and Engineering Southwest Jiaotong University Chengdu, Sichuan, 610031, China, Tel/Fax: +68 28 8760 0454, E-mail: s.grasso@swjtu.edu.cn

Keywords: Arc-melting, High entropy metal diborides, Hardness, Microstructure, X-ray diffraction

Abstract

High entropy metal diborides, a radically new approach to extend the chemical composition window of UHTCs, have been mainly processed using solid state sintering. In this work, arc-melting was used to produce dense high entropy metal diborides starting from powders. In order to understand the influence of each individual diboride, within the quinary system (HfB_2, ZrB_2, TiB_2, TaB_2 and CrB_2), we investigated five quaternary equimolar solid solutions *e.g.* Hf-Zr-Ti-Ta, Hf-Zr-Ti-Cr, Hf-Zr-Ta-Cr, Hf-Ti-Ta-Cr, Zr-Ti-Ta-Cr. Arc-melting allowed a rapid screening of favorable and unfavorable combinations. Unlike materials produced using solid state diffusion arc melting was able to produce samples free from undesired oxides. Because of CrB_2 evaporation during arc melting, it was hardly found in the solid solution; vapor pressure should be accounted when designing HEB compositions especially for operating temperatures exceeding 2000 ˚C. Vickers hardness showed clear drop for materials not containing TiB_2, which was attributed to its lattice mismatch effect.

1. Introduction

Borides and carbides of transition metals such as, ZrB_2, TiB_2, HfC, TaC, are known as ultra-high temperature ceramics (UHTCs). Owing to their particularly chemical and physical properties, high melting temperatures above ~3000 °C, excellent high temperature strengths, high hardness, good thermal and electrical conductivity and ablation resistance [1], UHTCs can be used in extreme temperatures and chemically aggressive environments. UHTCs are difficult to densify because of melting point resulting from strong covalent bonding [1,2]. Current UHTC applications in hypersonic flights and rocket propulsion have operation requirements exceeding bulk mono-phasic materials. Pure monolithic ceramics present a series of limitations, such as poor damage tolerance and critical oxidation resistance [3,4]. Several studies have demonstrated that combining UHTCs with other elements such as metals [5], carbides, borides, nitrides [6] and metal disilicides [7], can help to solve some of these major drawbacks.

In recent years, high entropy alloys (HEA) have attracted growing interest [8–10]. Starting from work on metals, these new alloys are composed of "*r*"-number of metal specimens, generally $r \geq 5$, to form a high entropy solution having increased entropy of mixing $\Delta S_{mix} = -nR \sum_{i=1}^{r} x_i \ln x_i$,where *n* is the total number of moles, *R* is the gas constant, x_i is the mole fraction of component *i* [9]. The theory supporting these new alloys relies upon the principle of Gibbs free energy minimization, $\Delta G = \Delta H - T \cdot \Delta S$. According to this principle, a system with an enhanced entropy (ΔS) is more stable ($\Delta G<0$) at high temperatures thanks to the contribution of the entropic term (-T·ΔS). HEAs have been shown to have improved properties compared to conventional alloys. Further necessary conditions for the existence of the substitutional solid solutions are set by the Hume-Rothery solid solution rules. Indeed, in order to obtain substitute alloys, two or more metals must meet the following requirements: 1) atomic radii that do not differ by more than 15 %, 2) same crystal structure, 3) similar electronegativity, 4) same valence.

Recently, high entropy oxides [11–14], borides [15–18], carbides [19–22] and silicides [23] have been obtained using different synthesis/sintering techniques such as spark plasma sintering and

pressureless sintering. For instance, Gild et al. [13] have successfully synthesized high-entropy fluorite oxides (HEFO), with hardness comparable to 8 mol. Y_2O_3-stabilized ZrO_2 and low electrical and thermal conductivities.

Castel et al. [20] have shown a significant enhancement in hardness of high entropy carbides material compared to the value calculated according to the rule of mixtures from the reference monocarbides and in comparison to the hardest monocarbide. Tallarita et al. [17] have produced high entropy borides starting from the respective oxides and boron, through a two-step processing method of Self-propagating High-temperature Synthesis (SHS) followed by the SPS. This approach avoided the need for intense mechanical milling of individual borides. Although reactive sintering by SPS may be faster than hot pressing and pressureless sintering, it still requires costly equipment, high temperatures (>2000 °C) and high pressures (tens of MPa) to promote atomic diffusion of different elements to obtain solid solutions.

Alternatively, Zhang et al. [24] have obtained solid solutions of binary and ternary carbides in a very short time (10-20 seconds) using the arc melting technique. This technique, already known in the metallurgical field, is able to reach very high temperatures, and therefore, melting materials with high melting point, close to 4000 °C, in a short time (a few seconds). In this way it was possible demonstrate the formation of solid solutions of binary, ternary carbides.

The aim of this work is to demonstrate the formation of high entropy borides (HEB), mixing equimolar composition of HfB_2, ZrB_2, TiB_2, TaB_2 and CrB_2, through the arc-melting technique. Moreover, since this technique allows rapid fabrication of large number of samples, we prepared 6 compositions (one quinary and five quaternaries) to study the effect of each single boride on the formation of HEB solid solution.

2. Experimental

Five commercial powders of transition metal diborides of HfB_2 (Treibacher, D_{50} 2.56 μm, impurities (wt.%): 0.23 C, 0.01 N, 0.23 O, <0.001 S), TaB_2 (Materion, purity 99.5%, impurities (wt.%): 0.04 Al, < 0.0007 Cd, < 0.0005 Cr, 0.07 Fe, 0.02 Nb, <0.0004 Pb), TiB_2 (H.C. Starck, Grade F, D_{90} 4.0 -7.0 μm, D_{50} 2.5-3.5 μm, impurities (wt. %): 0.4 C, 2.5 O, 0.5 N, 0.1 Fe), ZrB_2 (H.C. Starck, Grade B, D_{90} 4.0 -6.0 μm, D_{50} 1.5-3 μm, impurities (wt. %): 0.2 C, 1.5 O, 0.25 N, 0.1 Fe, 0.2 Hf), CrB_2 (H.C. Starck, Grade B, D_{90} 4.0 -6.0 μm, D_{50} 1.5-3 μm, impurities (wt. %): 0.3 C, 0.6 O, 0.5 Fe) were used to prepare six mixtures. One with all five equimolar elements and five equimolar combinations of 4 out of 5 borides: e.g (HfB_2, ZrB_2, TiB_2, TaB_2), (HfB_2, ZrB_2, TiB_2, CrB_2) (HfB_2, ZrB_2, CrB_2, TaB_2), (HfB_2, CrB_2, TiB_2, TaB_2), (CrB_2, ZrB_2, TiB_2, TaB_2). The six compositions are listed in Table 1. The starting equimolar powders were mixed by dry milling in a polyethylene bottle for 24h. All mixtures were subjected with a pre-sintering cycle by Spark plasma sintering furnace (Chenhua 10–20 SPS furnace (China)), at 1600 °C under a pressure of 25 MPa, heating rate of 80 °C/min and dwelling time of 10 minutes, in order to clean borides from oxide impurities as much as possible. From each of the 6 pre-sintered pellets, 10 smaller pieces with a volume of about 40 mm^3 were obtained for the arc-melting experiments in order to have similar heating and cooling rates.

All samples were melted on a water-cooled copper crucible using arc melting by TIG-200P (AC/DC) (Dongguan Hanhuang Welding and Cutting Equipment Co., Ltd, China) under argon flow, with purity of 99.999 %, applying a current of 100 A for 10-20 seconds. The argon flow was maintained for 10 seconds after switching off the current in order to protect the samples from the oxidation during the free cooling. The samples were re-melted 5 times in order to homogenize as much possible the mixture during the formation of the melt.

The microstructure was analyzed on polished cross section, using diamond discs up to 0.25 μm, by field-emission scanning electron microscopy (FESEM, mod. ΣIGMA, ZEISS NTS Gmbh,

Oberkochen, Germany) equipped with energy X-ray dispersive microanalysis (EDS, Model INCA energy 300; Oxford Instruments, UK). Crystalline phases of the samples, obtained from the melt, were identified by X-ray diffraction (XRD, mod. D8 Advance - Bruker, Germany) with Cu Kα radiation, step size of 0.04 and 0.5 s counting rate in the 20–100° 2θ range. The hardness was measured by Vickers indentation method applied a load of 1.96 N (200 g), 4.90 N (500 g) and 9.8 N (1000 g) (Innovatest Falcon 505, Rupac, Netherlands) for 15 seconds.

Table 1. Quantitative Experimental results of EDS mapping of inner part of the samples

	Sample	Hf	Zr	Ti	Ta	Cr	Equimolar elements*
		Atomic %					
1- all borides	**$(Hf_{0.20}, Zr_{0.20}, Ti_{0.20}, Ta_{0.20}, Cr_{0.20})B_2$**	25	22	23	27	1	Hf, Zr, Ti, Ta
2-CrB_2	**$(Hf_{0.25}, Zr_{0.25}, Ti_{0.25}, Ta_{0.25})B_2$**	27	24	22	25	-	Hf, Zr, Ti, Ta
3-TaB_2	**$(Hf_{0.25}, Zr_{0.25}, Ti_{0.25}, Cr_{0.25})B_2$**	39	30	30	-	1	Hf, Zr, Ti
4-TiB_2	**$(Hf_{0.25}, Zr_{0.25}, Cr_{0.25}, Ta_{0.25})B_2$**	32	30	-	36	0.8	Hf, Zr, Ta
5-ZrB_2	**$(Hf_{0.25}, Cr_{0.25}, Ti_{0.25}, Ta_{0.25})B_2$**	37	-	29	31	2	Hf, Ti, Ta
6-HfB_2	**$(Cr_{0.25}, Zr_{0.25}, Ti_{0.25}, Ta_{0.25})B_2$**	-	33	32	33	1	Zr, Ti, Ta

***error within 3% measured using EDS**

3. Results and discussion

3.1 X-ray diffraction spectra.

Fig. 1 shows X-ray diffraction spectra: all samples display the primitive hexagonal unit cell typical of the isomorphous starting diborides. Principal diffractions are usually surrounded by smaller peaks, which accounts for phase separation discussed in sections 3.2 and 3.4.

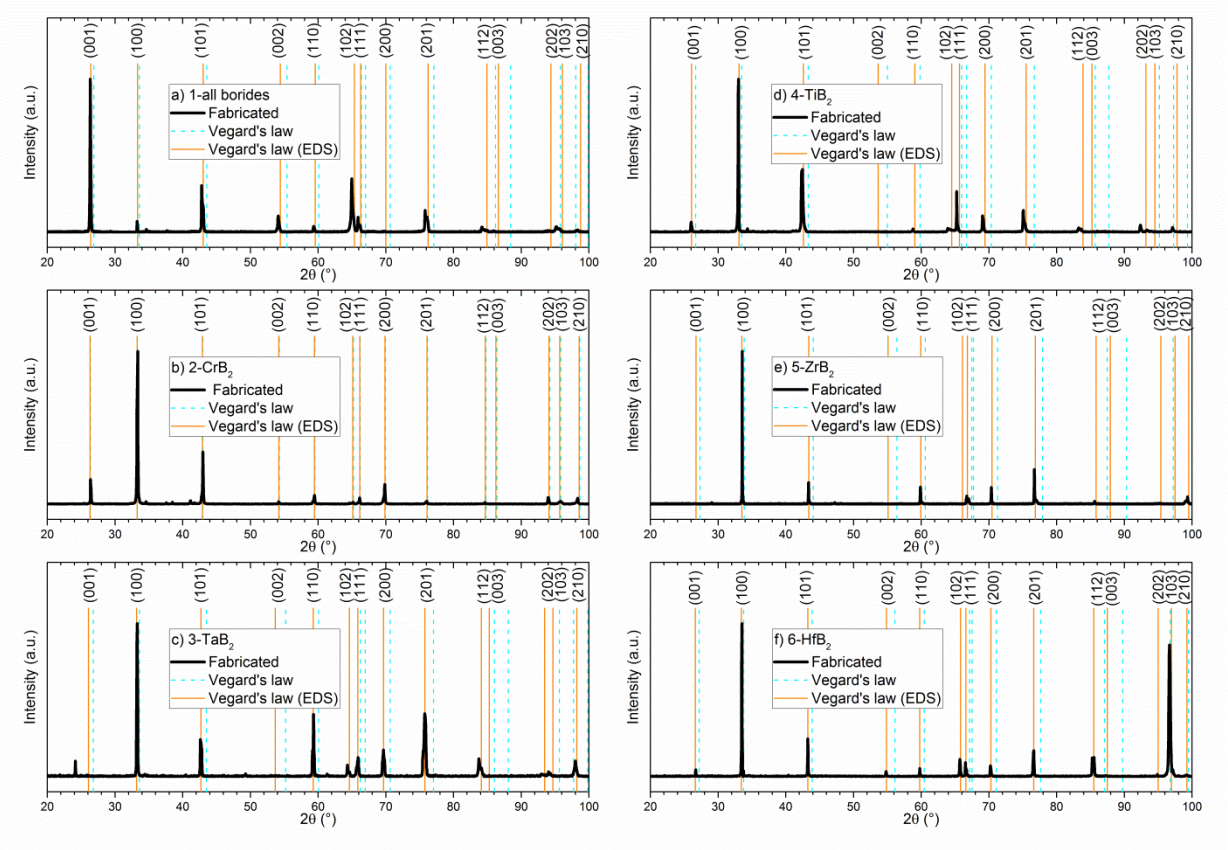

Figure 1: X-ray diffraction patterns for the 6 mixtures and reference spectra of expected borides.

Nevertheless, considering main peaks ascribed to hexagonal phase, lattice parameters obtained from XRD patterns are shown in Table 2 together with that calculated by means of Vergard's rule [25]. The calculation of the lattice parameters was done using reference lattice parameters (PDF card n. 65-0878, 65-1037, 65-1883, 65-3389, and 65-3387 for TaB_2, TiB_2, CrB_2, HfB_2, ZrB_2, respectively), and the data of at% obtained by EDS analysis explained below. As it can be seen form the Fig. 1, the deviation from Vegard's rule is minimized if composition measured by EDS analysis is taken into account instead of the starting equimolar composition. As for diborides and binary diborides solid solutions, lattice parameters vary linearly with the mean size of the metal atoms (Fig. 2).

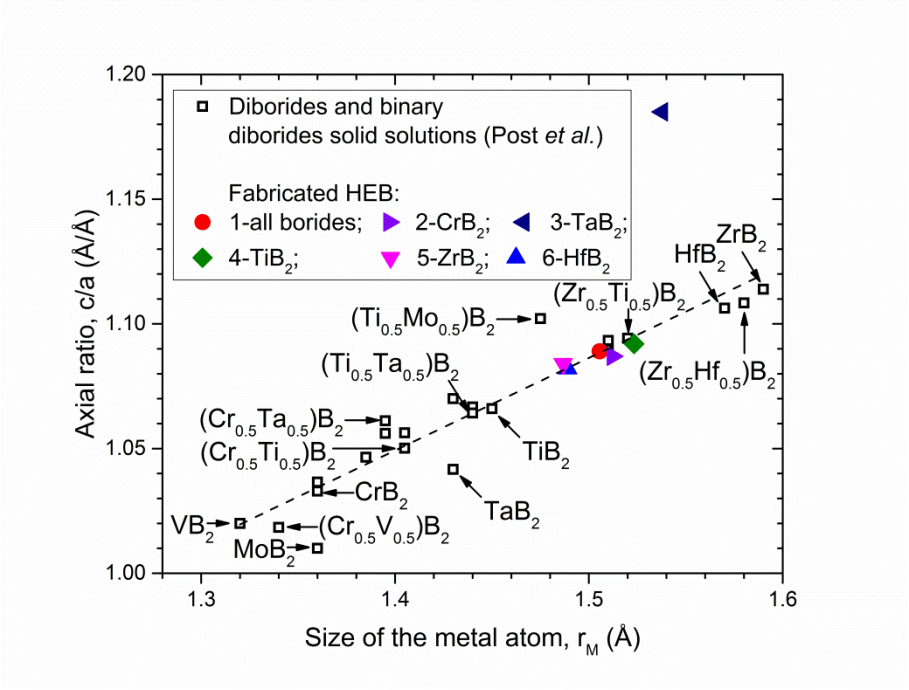

Figure 2: c/a ratio vs. atomic radii of metal atom, r_m.

The anomalous *c*/*a* variation of 3-TaB_2 solid solution is far more pronounced than that of $(Ti_{0.5}Mo_{0.5})B_2$ observed by Post et al. [26]. The reason of the large deviation of about 8% in the length of the *c*-axis is difficult to determine. However, this result suggests that (i) there is a negligible, or no, amount of Cr in solid solution, and (ii) metal-to-metal replacement to form solid solution occurred readily in the Hf, Zr, Ti, and Ta diborides.

Table 2. Lattice constants *a*, and *c* (Å) obtained from observed (100) and (001) peaks, respectively, compared to the one calculated using Vergard's rule. *c* values of sample 5 were extrapolated from (101) peak.

	a XRD	*a* Vergard	*c* XRD	*c* Vergard	*c*/*a* XRD	*c*/*a* Vergard
1- all borides	3.109	3.102	3.387	3.370	1.089	1.086
2-CrB_2	3.101	3.107	3.372	3.382	1.087	1.089
3-TaB_2	3.107	3.115	3.683	3.413	1.185	1.096
4-TiB_2	3.132	3.125	3.421	3.415	1.092	1.093
5-ZrB_2	3.082	3.085	3.340	3.330	1.084	1.080
6-HfB_2	3.086	3.091	3.338	3.344	1.082	1.082

3.2 Sample morphology and EDS analysis

Fig. 3 shows the cross section of the samples obtained from the arc-melting process of the six materials listed in Table 1.

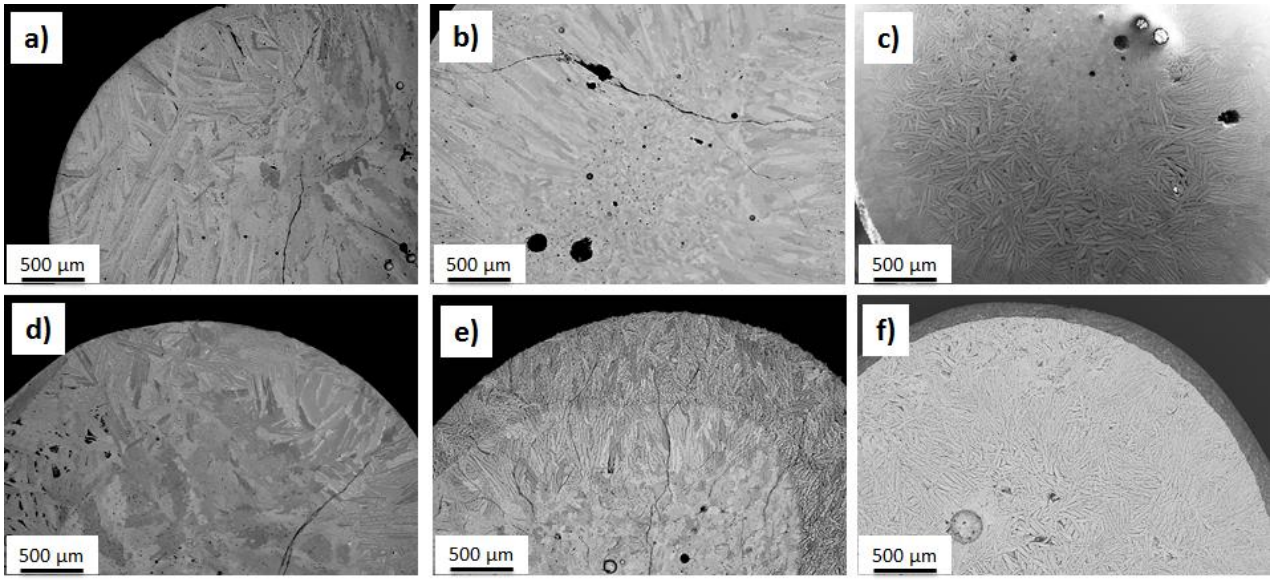

Figure 3. Cross section of spherical HEB samples: a) 1- all, b) 2- CrB_2, c) 3- TaB_2, d) 4- TiB_2, e) 5- ZrB_2, f) 6- HfB_2.

All materials are completely dense, with the exception of 4, missing TiB_2, that exhibited small distributed porosity in the center and voids in the edges (see supplementary section). Most of them were found to be affected by cracks due thermal shock/strong temperature gradient experienced during arc-melting treatment. They all exhibited the typical anisotropic microstructure of metallic materials obtained from melting [27,28]. During cooling down, the surface cooled much faster than the core, which generated a strong radial temperature gradient. As a result, an anisotropic structure was created, with rounded/coarsened grains in the (hot) core that gradually changed to elongated and dendritic-like grains towards the rapidly cooling surface. Approximately, the transition from rounded to elongated grains occurred at a distance of 2 mm from the center. According to EDS analyses, a single solid solution phase was detected in the core grains constituting the inner part of the molten samples, in agreement with the phases detected by X-ray diffraction and in agreement

with the large mutual solubility range of diborides observed by other authors [29]. Moreover, grain boundaries are clean in this portion of material. Shifting from the core to the edge, compositions and morphology of the grains changed and liquid phase separation was observed in the grain boundary regions.

In all the compositions containing Cr, Cr was preferentially detected along the grain boundary as a secondary phase, though a tiny percentage was also found in solid solution (see quantitative analyses in Table 1). Indeed, observing the EDS compositional maps of sample 1-all borides ($Hf_{0.20}$, $Zr_{0.20}$, $Ti_{0.20}$, $Ta_{0.20}$, $Cr_{0.20}$)B_2, in Fig. 4, and except those contain Cr, they presented a quasi-equimolar solid solution of HfB_2, ZrB_2 TiB_2 and TaB_2 formed. This fact is even more evident in sample 2-CrB_2 where CrB_2 was not included the original mixture.

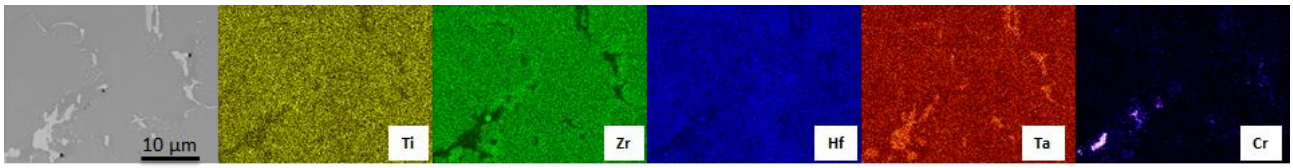

Figure 4. EDS compositional maps of inner part of the sample 1-all borides, containing all elements. A complete solid solution formed while CrB_2 resulted in phase separation.

Noteworthy, in sample 2-CrB_2 ($Hf_{0.25}$, $Zr_{0.25}$, $Ti_{0.25}$, $Ta_{0.25}$) B_2, missing Cr, Ta segregation between the grains was observed as shown in Fig 5 b).

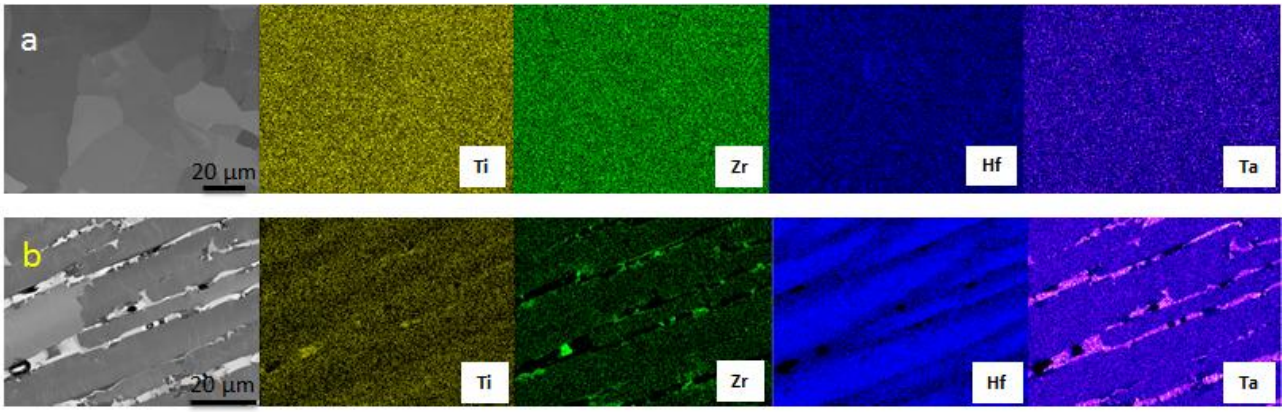

Figure 5. EDS compositional maps of a) inner part and b) external part of the sample 2-CrB_2.

For mixtures 3, 4, 5 and 6, figures are reported in the supplementary material. Sample 3, ($Hf_{0.25}$, $Zr_{0.25}$, $Ti_{0.25}$, $Cr_{0.25}$)B_2 was characterized by a solid solution with almost equal atomic content of Hf, Zr, and Ti, but much smaller content of Cr. Cr was preferentially detected at the grain boundaries. Towards the edge of the pellet, we noticed that elongated grains composed of Hf, Zr, and Ti were surrounded by ZrB_2 rounded agglomerates and CrB_2 phases (see Fig. A1 a) and b)).

Similarly, Sample 4 ($Hf_{0.25}$, $Zr_{0.25}$, $Cr_{0.25}$, $Ta_{0.25}$)B_2, displayed rather clean grain boundaries in the center, with small CrB_2 –based secondary phases at the grain boundaries. On the contrary, going towards the edge, elongated grains were surrounded by mixed separated phase with irregular morphology (see Fig. A2 a) and b)). Samples 5 ($Hf_{0.25}$, $Cr_{0.25}$, $Ti_{0.25}$, $Ta_{0.25}$)B_2 and 6 ($Cr_{0.25}$, $Zr_{0.25}$, $Ti_{0.25}$, $Ta_{0.25}$)B_2, showed the same characteristics (see Fig. A3 a) and b) and A4 a) and b)).

3.3 Hardness

Indentations were collected indistinctly in the central and close to the edge of the samples. Values were in the range 19-20 GPa, and slightly increased to 20-23 GPa reducing the load from 1 to 0.5 and 0.2 Kg, shown in Fig. 6 and Table 2A mainly due to the indentation size effect [30], [31].

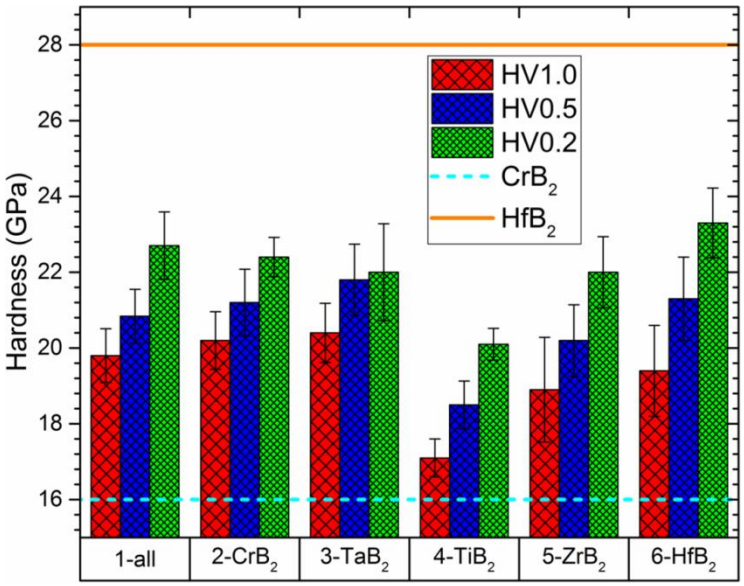

Figure 6. Hardness value measured with load 1, 0.5 and 0.2 Kg for quaternary and quinary borides. HfB_2 and CrB_2 lines are the hardest and softest borides as reference materials such indicated by Fahrenholtz et al. [1] and Mahesh et al. [32]

The lowest values were found for the mixture without TiB_2, a feature which can be attributed to residual porosity shown in figure 3 d) . Amongst the other fully dense mixtures, the hardest one was sample 3, missing TaB_2 probably due to its finer microstructure. Table 1A shows physical and chemical properties of the transition metal diborides considered in this work. They all satisfy the Hume-Rothery solid solution rule, as demonstrated by [15].

3.4 Microstructural evolution

In their work, Gild et al. [15], demonstrated the formation of a high entropy phase including CrB_2 using the spark plasma sintering technique, despite the limited solid solubility of CrB_2 in both HfB_2 and ZrB_2 [26]. In our case, the formation of high entropy diboride should be easier because, in the molten state, the activation energy for diffusion is much smaller than in the solid state [33]. Compared to the starting compositions we observed a reduction in the content of CrB_2 in all mixtures and TaB_2 in the case of 5-CrB_2, (e.g. when Chromium boride was not included). Indeed,

we hypothesized that in the arc melting process, formation of solid solutions is not just affected by the melting points of each individual material, but also by vapor partial pressure of each constituent. In this work, CrB_2 has the highest vapor partial pressure followed by TaB_2, shown in Table 1A at relative melting point. Therefore, in samples containing CrB_2 (1, 3, 4, 5, 6) the peculiar microstructure obtained is affected by the fast vaporization and evaporation of CrB_2 from the center towards the surface. To a lower extent, TaB_2 also experienced the same phenomenon, because of its high vapor partial pressure. Broadly, microstructural evolution of compositions containing CrB_2 can be schematized as follows. During heating:

1) at least 2 melts form, with different melting points and composition. Since CrB_2 melting point << other borides, at temperature around 2000°C or below CrB_2 becomes liquid and partially dissolves other borides in the vicinity, forming the L1 liquid phase.
2) As the temperature continues to rise and melting proceeds towards the pellet interior, new L1 liquid phase is formed and evaporation of CrB_2 occurs on the surface.
3) Other molten liquids form (L2, with no CrB_2), with higher melting point than L1.
4) Progressive/fast extension of melting from the surface down to the core and progressive depletion of CrB_2 from the core

During cooling:

1) the solid solution nuclei from L2 (most refractory) liquid type begin to solidify from the outer surface and grow forming columnar grains that develop in the direction of the temperature gradient present in the sample. These crystalline nuclei are mainly formed by solid solutions of the high melting elements, where HfB_2, ZrB_2, TiB_2 are quasi equimolar whilst TaB_2 is slightly lower due to partial evaporation.
2) CrB_2 vaporization is blocked in the proximity of the outer surface due to rapid closure of exit channels and the CrB_2-liquid phase (L1) remains trapped and solidifies along the grain boundaries, as observed by SEM-EDS.

3) CrB_2 secondary melt separation occurs because of different factors, including its reduced melting point compared to other borides, decreased solubility of other borides when the temperature decreases and extremely fast cooling (≈1000 ˚C/s).

Finally, in sample 2, missing CrB_2, TaB_2 is the lowest melting temperature phase, thus in this case, TaB_2 based liquid phase is formed and phase separation mainly involving TaB_2 occurs during cooling.

Mechanisms occurring during cooling are sketched in Fig. 7.

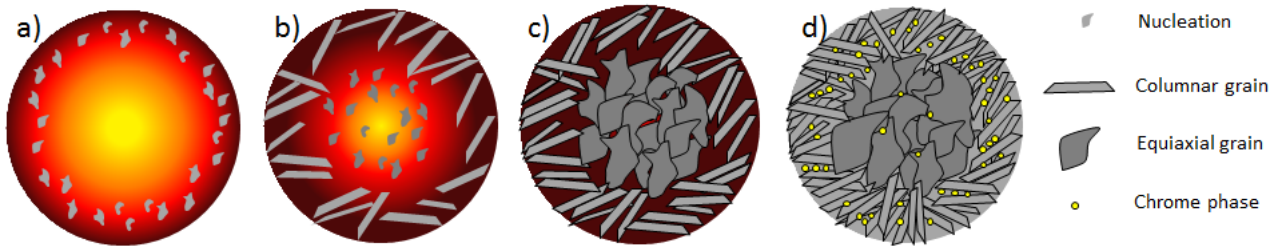

Figure 7. Solidification mechanism: a) first formation of crystalline nuclei in the outermost area formed by the high melting elements (HfB_2, ZrB_2, TiB_2, TaB_2), b) nuclei growth forming columnar grains that develop in the direction of the temperature gradient and formation of crystalline nuclei in the central part of the sample c) growth of the equiaxial grains in the innermost area of the material formed by an equimolar solid solution d) precipitation of Cr element among the grain boundary principally in the external part of the sample

Finally, future work is concerned with additional experiments to control the cooling rate. It is expected that producing larger samples has the effect to decrease the cooling rate, limiting or suppressing the formation of a core – shell structure, with the dense equiaxed core and elongated shell grains. This could be achieved by lowering gradually the arc current or using a heated stage.

4. Conclusions

High entropy metal diborides were obtained using the arc-melting technique staring from a powder mixture. HfB_2, ZrB_2, TiB_2 and TaB_2 formed equimolar solid solutions as confirmed by EDS analysis. Unlike solid state processing, the similarity in melting point and vapor partial pressure of each individual diboride is an essential requirement to achieve homogenous samples using arc-melting technique. CrB_2 did not form a solid solution because during processing its low melting point contributed to phase separation while its high vapor partial pressure induced almost complete sublimation. The XRD analysis confirmed that, in each samples, were not present oxide phases and the values of lattice parameters were in agreement with theoretical values. The influence of each element on the hardness values showed no large variations and lowest value was for the sample without TiB_2. The results obtained in this work demonstrates as arc-melting technique could allow a rapid screening of hundreds of high entropy borides compositions avoiding long reaction times needed in solid state processing.

Acknowledgments

The authors would like to thank M. Mazzocchi (ISTEC-CNR, Italy) for assistance with XRD analysis. This research did not receive any specific grant from funding agencies in the public, commercial, or not-for-profit sectors

References

[1] W.G. Fahrenholtz, G.E. Hilmas, I.G. Talmy, J.A. Zaykoski, Refractory diborides of zirconium and hafnium, J. Am. Ceram. Soc. 90 (2007) 1347–1364. doi:10.1111/j.1551-2916.2007.01583.x.

[2] J.K. Sonber, A.K. Suri, Synthesis and consolidation of zirconium diboride: review, Adv. Appl. Ceram. 110 (2011) 321–334. doi:10.1179/1743676111y.0000000008.

[3] T.A. Parthasarathy, R.A. Rapp, M. Opeka, R.J. Kerans, A Model for Transitions in Oxidation

Regimes of ZrB2, Mater. Sci. Forum. 595–598 (2008) 823–832. doi:10.4028/www.scientific.net/MSF.595-598.823.

[4] T.A. Parthasarathy, R.A. Rapp, M. Opeka, R.J. Kerans, A model for the oxidation of ZrB_2, HfB_2 and TiB_2, Acta Mater. 55 (2007) 5999–6010. doi:10.1016/j.actamat.2007.07.027.

[5] H. Wang, D. Chen, C.A. Wang, R. Zhang, D. Fang, Preparation and characterization of high-toughness ZrB_2/Mo composites by hot-pressing process, Int. J. Refract. Met. Hard Mater. 27 (2009) 1024–1026. doi:10.1016/j.ijrmhm.2009.06.003.

[6] F. Monteverde, A. Bellosi, S. Guicciardi, Processing and properties of zirconium diboride-based composites, J. Eur. Ceram. Soc. 22 (2002) 279–288. doi:10.1016/S0955-2219(01)00284-9.

[7] L. Silvestroni, S. Failla, I. Neshpor, O. Grigoriev, Method to improve the oxidation resistance of ZrB2 -based ceramics for reusable space systems, J. Eur. Ceram. Soc. 38 (2018) 2467–2476. doi:10.1016/j.jeurceramsoc.2018.01.025.

[8] J.W. Yeh, S.K. Chen, S.J. Lin, J.Y. Gan, T.S. Chin, T.T. Shun, C.H. Tsau, S.Y. Chang, Nanostructured high-entropy alloys with multiple principal elements: Novel alloy design concepts and outcomes, Adv. Eng. Mater. 6 (2004) 299-303+274. doi:10.1002/adem.200300567.

[9] Y. Zhang, T.T. Zuo, Z. Tang, M.C. Gao, K.A. Dahmen, P.K. Liaw, Z.P. Lu, Microstructures and properties of high-entropy alloys, Prog. Mater. Sci. 61 (2014) 1–93. doi:10.1016/j.pmatsci.2013.10.001.

[10] M.H. Tsai, J.W. Yeh, High-entropy alloys: A critical review, Mater. Res. Lett. 2 (2014) 107–123. doi:10.1080/21663831.2014.912690.

[11] C.M. Rost, E. Sachet, T. Borman, A. Moballegh, E.C. Dickey, D. Hou, J.L. Jones, S.

Curtarolo, J.P. Maria, Entropy-stabilized oxides, Nat. Commun. 6 (2015) 1–8. doi:10.1038/ncomms9485.

[12] S. Jiang, T. Hu, J. Gild, N. Zhou, J. Nie, M. Qin, T. Harrington, K. Vecchio, J. Luo, A new class of high-entropy perovskite oxides, Scr. Mater. 142 (2018) 116–120. doi:10.1016/j.scriptamat.2017.08.040.

[13] J. Gild, M. Samiee, J.L. Braun, T. Harrington, H. Vega, P.E. Hopkins, K. Vecchio, J. Luo, High-entropy fluorite oxides, J. Eur. Ceram. Soc. 38 (2018) 3578–3584. doi:10.1016/j.jeurceramsoc.2018.04.010.

[14] M. Biesuz, S. Fu, J. Dong, A. Jiang, D. Ke, Q. Xu, D. Zhu, M. Bortolotti, M.J. Reece, C. Hu, S. Grasso, High entropy $Sr((Zr_{0.94}\ Y_{0.06})_{0.2}\ Sn_{0.2}\ Ti_{0.2}\ Hf_{0.2}\ Mn_{0.2}\ )O_{3-x}$ perovskite synthesis by reactive spark plasma sintering, J. Asian Ceram. Soc. 0 (2019) 1–6. doi:10.1080/21870764.2019.1595931.

[15] J. Gild, Y. Zhang, T. Harrington, S. Jiang, T. Hu, M.C. Quinn, W.M. Mellor, N. Zhou, K. Vecchio, J. Luo, High-Entropy Metal Diborides: A New Class of High-Entropy Materials and a New Type of Ultrahigh Temperature Ceramics, Sci. Rep. 6 (2016) 2–11. doi:10.1038/srep37946.

[16] P.H. Mayrhofer, A. Kirnbauer, P. Ertelthaler, C.M. Koller, High-entropy ceramic thin films; A case study on transition metal diborides, Scr. Mater. 149 (2018) 93–97. doi:10.1016/j.scriptamat.2018.02.008.

[17] G. Tallarita, R. Licheri, S. Garroni, R. Orrù, G. Cao, Novel processing route for the fabrication of bulk high-entropy metal diborides, Scr. Mater. 158 (2019) 100–104. doi:10.1016/j.scriptamat.2018.08.039.

[18] Y. Zhang, Z.-B. Jiang, S.-K. Sun, W.-M. Guo, Q.-S. Chen, J.-X. Qiu, K. Plucknett, H.-T.

Lin, Microstructure and mechanical properties of high-entropy borides derived from boro/carbothermal reduction, J. Eur. Ceram. Soc. (2019) 0–1. doi:10.1016/j.jeurceramsoc.2019.05.017.

[19] J. Dusza, P. Švec, V. Girman, R. Sedlák, E.G. Castle, T. Csanádi, A. Kovalčíková, M.J. Reece, Microstructure of (Hf-Ta-Zr-Nb)C high-entropy carbide at micro and nano/atomic level, J. Eur. Ceram. Soc. 38 (2018) 4303–4307. doi:10.1016/j.jeurceramsoc.2018.05.006.

[20] E. Castle, T. Csanádi, S. Grasso, J. Dusza, M. Reece, Processing and Properties of High-Entropy Ultra-High Temperature Carbides, Sci. Rep. 8 (2018) 1–12. doi:10.1038/s41598-018-26827-1.

[21] X. Yan, L. Constantin, Y. Lu, J.F. Silvain, M. Nastasi, B. Cui, $(Hf_{0.2}\ Zr_{0.2}\ Ta_{0.2}\ Nb_{0.2}\ Ti_{0.2})C$ high-entropy ceramics with low thermal conductivity, J. Am. Ceram. Soc. 101 (2018) 4486–4491. doi:10.1111/jace.15779.

[22] P. Sarker, T. Harrington, C. Toher, C. Oses, M. Samiee, J.P. Maria, D.W. Brenner, K.S. Vecchio, S. Curtarolo, High-entropy high-hardness metal carbides discovered by entropy descriptors, Nat. Commun. 9 (2018) 1–10. doi:10.1038/s41467-018-07160-7.

[23] J. Gild, J. Braun, K. Kaufmann, E. Marin, T. Harrington, P. Hopkins, K. Vecchio, J. Luo, A high-entropy silicide: $(Mo_{0.2}Nb_{0.2}Ta_{0.2}Ti_{0.2}W_{0.2})Si2$, J. Mater. (2019). doi:10.1016/j.jmat.2019.03.002.

[24] Z. Zhang, S. Fu, F. Aversano, M. Bortolotti, H. Zhang, C. Hu, S. Grasso, Arc melting: a novel method to prepare homogeneous solid solutions of transition metal carbides (Zr, Ta, Hf), Ceram. Int. 45 (2019) 9316–9319. doi:10.1016/j.ceramint.2019.01.238.

[25] A.R. Denton, N.W. Ashcroft, Vergard's law, Phys. Rev. A. 43 (1991). doi:https://doi.org/10.1103/PhysRevA.43.3161.

[26] B. Post, F.W. Glaser, D. Moskowitz, Transition metal diborides, Acta Metall. 2 (1954) 20–25. doi:10.1016/0001-6160(54)90090-5.

[27] H. Biloni, B. Chalmers, Origin of the equiaxed zone in small ingots, J. Mater. Sci. 3 (1968) 139–149. doi:10.1007/BF00585481.

[28] G.S. Cole, Inhomogeneities and their control via solidification, Metall. Trans. 2 (1971) 357–370. doi:10.1007/BF02663323.

[29] S. Otani, T. Aizawa, N. Kieda, Solid solution ranges of zirconium diboride with other refractory diborides: HfB_2, TiB_2, TaB_2, NbB_2, VB_2 and CrB_2, J. Alloys Compd. 475 (2009) 273–275. doi:10.1016/j.jallcom.2008.08.023.

[30] K. Sangwal, Review: Indentation size effect, indentation cracks and microhardness measurement of brittle crystalline solids - some basic concepts and trends, Cryst. Res. Technol. 44 (2009) 1019–1037. doi:10.1002/crat.200900385.

[31] A. Krell, A new look at grain size and load effects in the hardness of ceramics, Mater. Sci. Eng. A. 245 (1998) 277–284. doi:10.1016/S0921-5093(97)00724-7.

[32] B. Mahesh, K. Sairam, J.K. Sonber, T.S.R.C. Murthy, G.V.S. Nageswara Rao, T. Srinivasa Rao, J.K. Chakravartty, Sinterability studies of monolithic chromium diboride (CrB_2) by spark plasma sintering, Int. J. Refract. Met. Hard Mater. 52 (2015) 66–69. doi:10.1016/j.ijrmhm.2015.04.035.

[33] J.R. Cahoon, Modified “hole” theory for solute impurity diffusion in liquid metals, Metall. Mater. Trans. A Phys. Metall. Mater. Sci. 28 A (1997) 583–593. doi:10.1007/s11661-997-0044-3.